JOURNAL OF Applied Polymer SCIENCE

Effects of the Film Thickness on the Morphology, Structure, and Crystal Orientation Behavior of Poly(chloro-*p*-xylylene) Films

Kaiyuan Tan, Hao Zhang, Maoping Wen, Ziwei Du
Institute of Chemical Materials, China Academy of Engineering Physics, Mianyang, Sichuan 621900, People's Republic of China
Correspondence to: K. Tan (E-mail: tanky@caep.cn)

ABSTRACT: Poly(chloro-*p*-xylylene) (PPXC) films with a thickness range encompassing more than three orders of magnitude (from 10^2 nm to 10^2 μm) were prepared on Si substrates by the chemical vapor deposition method under the same conditions. The effect of the film thickness (d) on the morphology, crystal structure, and crystal orientation behavior of the PPXC films was studied. The average roughness of the root mean square (rms) of the films increased with increasing d according to a power law (rms $\approx d^{\beta}$, where β is an exponent that depends on the film growth process over time and $\beta = 0.240 \pm 0.005$, as probed by atomic force microscopy), and the monomer diffusion and relaxation of polymer were suggested as the primary factors governing this morphological evolution. The X-ray diffraction results indicate that both the crystallinity and crystal size of PPXC increased with increasing d due to the surface confinement effect between the film and the substrate, which retarded the crystallization process. The X-ray pole figures suggested that the (020) fiber textures with the b axis parallel to the Si substrate normal existed in the PPXC films; these fiber textures, mainly composed of edge-on crystal lamellae, were thermodynamically favored. The Herman's orientation factor of the fiber textures increased gradually as d grew; this indicated that stronger (020) fiber textures with higher concentrations of edge-on lamellae existed in the thicker PPXC films. This thickness dependence of the crystal orientation behavior was interpreted to be caused by the strong adhesion between the polymer chains and the substrate. © 2014 Wiley Periodicals, Inc. J. Appl. Polym. Sci. **2015**, *132*, 41394.

KEYWORDS: biomaterials; films; morphology; X-ray

Received 2 March 2014; accepted 8 August 2014
DOI: 10.1002/app.41394

INTRODUCTION

Poly(*p*-xylylene) (PPX) and its derivatives, known by the trade name Parylene, have attracted considerable scientific attention because of their outstanding properties, which include a high chemical resistance and thermal stability, low moisture sorption, low dielectric constant, good biocompatibility, and the fact that they can form uniform coatings on substrates of varied geometric shapes by vapor deposition.[1–5] Poly(chloro-*p*-xylylene) (PPXC or Parylene C) is one of the most widely used PPX derivative; it only differs from PPX in that its monomer has a chlorine atom substituted on the phenyl ring. PPXC has a higher thermooxidative stability than PPX; it also exhibits unique mechanical properties and inertness.[6] With their exceptional properties, PPXC films find a broad range of uses, such as protective coatings, moisture barriers, capacitor dielectrics, and many other advanced applications in microelectromechanical systems and biomedical areas.[6–11]

Parylene polymers are semicrystalline thermoplastics and are often synthesized as thin films by the chemical vapor deposition (CVD) method. The deposition conditions (deposition temperature, pressure, substrate, and so on) consequently play crucial roles in the morphology, microstructure, and properties of the films.[12–17] However, some other factors, such as the thermal history of the polymer films, can also severely influence the degree of crystallization, crystallite size, stress state, and thermal stability of the films.[13,14] Furthermore, because Parylene films with various thicknesses in a broad range are used in many different fields; the effect of the thickness on their structure is another important aspect that should be taken into great consideration. Pioneering works have shown that various scaling behaviors can exist for thin polymer films.[18–20] For Parylene polymers, several studies have reported that even under fixed deposition conditions, changes in the morphology, density, and crystallinity of Parylene films occurred as a function of the film thickness (d); these influence the hydrophobicity, glass-transition temperature, and dielectric and electrical properties of the as-deposited films.[21–24] However, most of these studies have focused on the film's morphology; other structural aspects, especially the crystal orientation behavior, have not been adequately addressed. You et al.'s[25] study indicated that the PPX films exhibited fiber texture structures, yet they did not focus on the effect of d on the

© 2014 Wiley Periodicals, Inc.

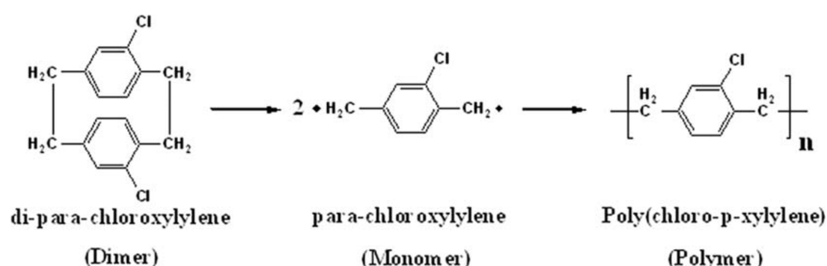

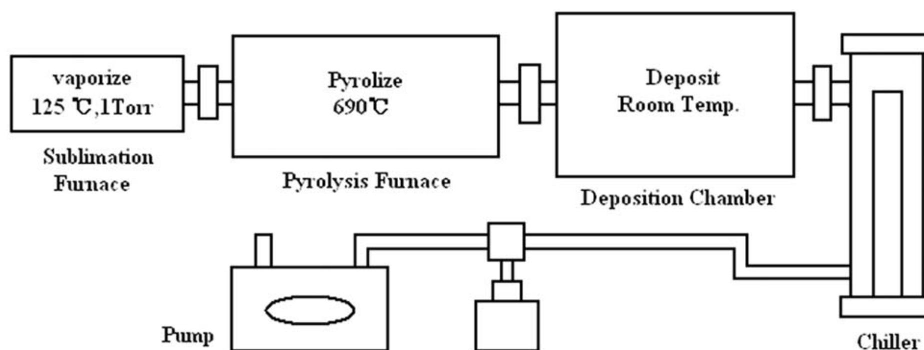

Figure 1. Scheme of the PPXC deposition process.

fiber texture, and PPXC films were not discussed. Because the semicrystalline PPXC films are widely used, the preferred orientation of the crystallites in PPXC films plays a crucial role in their many physical properties.[26] Therefore, more detailed knowledge of the microstructures of PPXC films is needed; this includes knowledge of their crystal orientation, crystallite aggregations, and polymer chain packing within the crystallites. In this study, PPXC films with thicknesses ranging from 10^2 nm to 10^2 μm were deposited under the same conditions by the CVD method; the effects of d on the morphology, crystalline structure, and especially the crystal orientation behavior of PPXC films were investigated.

EXPERIMENTAL

Materials

All solvents were purchased from Nanjing Chemical Reagent Co., Ltd. (Nanjing, China) and were used as received. The Parylene used in this study, a powder type of dimer di-*para*-chloroxylylene, was supplied from Penta Technology Co., Ltd. (Suzhou, China). The deposition substrate was a silicon wafer. Before deposition, the silicon substrates were cleaned twice with acetone and dried for 1 h at 70°C *in vacuo*.

Deposition of the PPXC Films

PPXC films were deposited by the well-known Gorham method[1] with a chemical deposition system for Parylene (PDS-2060PC, SCS). As shown in Figure 1, the deposition processes consisted of three steps:

1. Sublimation *in vacuo* at 1 Torr and approximately 125°C of the stable crystalline dimer di-*para*-chloroxylylene to produce vapors of this material.
2. Pyrolysis of the vapors at approximately 690°C to form gaseous *para*-chloroxylylene, the reactive monomer.
3. Deposition and simultaneous polymerization of the *para*-chloroxylylene at room temperature to form the PPXC film on an Si wafer.

During deposition, the pressure is typically in the low-milli-Torr range. The growth process was monitored by a quartz microbalance, which also provided a nominal d.[27,28] By changing the initial amount of Parylene dimer, we prepared five samples with different thicknesses under almost the same conditions.

Film Characterization

d was determined after preparation by a Veeco Detak150 surface profilometer (Veeco Metrology, Inc., CA) as the average of three measurements across a step.

The surface morphology was investigated by atomic force microscopy (AFM) with an SPA-300HV AFM instrument (Seiko Instruments, Inc., Japan). Height and phase images were acquired under ambient conditions in tapping mode. The average roughness of the root mean square (rms) was extracted from height images with dimensions of 5 × 5 μm^2 by the use of Nanonavi software.

The crystallinity and crystal structures of the films were investigated by high-resolution X-ray diffraction (XRD) in the BL14B X-ray beamline station at the Shanghai Synchrotron Radiation Facility (SSRF). The diffractometer was a Huber 5021 six-circle system with high precision with a 0.0001° step size for the 2θ circles. The measurements were carried out at room temperature with the following parameters: wavelength of the X-ray = 1.239 Å, scan range = 5–40°, and scan step size = 0.02°.

The wide-angle XRD experiment was carried out in transmission mode with the X-ray beam perpendicular to the film surface. The diffraction pattern was recorded by a Mar345 image plate detector, which stood behind the sample.

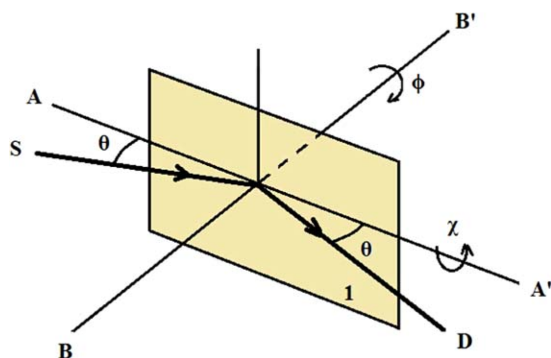

Figure 2. Schultz reflection pole figure geometry: (1) film surface, (S) X-ray beam, and (D) X-ray detector. [Color figure can be viewed in the online issue, which is available at wileyonlinelibrary.com.]

The X-ray pole figure was used to study the crystal orientation in the films (see Figure 2); this configuration is known as the *Schultz reflection method*.[29–32] To perform an X-ray pole figure scan with this method, the X-ray 2θ was first fixed with respect to one of the crystal planes of the sample (the major diffraction peak determined by XRD is normally chosen). The sample is then tilted about the AA′ axis from 0°, which corresponds to the usual 2θ scan position, as shown in Figure 2, to 90° [tilted angle (χ)] at periodic intervals; it is concurrently rotated about its surface normal (BB′ axis) from 0 to 360° [sample rotation (φ)] at each χ (for a uniaxial symmetric orientation sample, no rotation is necessary, only tilting from 0 to 90°). The detector collects the diffraction signals from the crystal planes corresponding to the set 2θ. Because 2θ does not change during the scan, XRD, therefore, gives the crystal plane normal (pole) distributions inside the film.

RESULTS AND DISCUSSION

d Measurement

The nominal thickness given by the quartz microbalance during the sample preparation is often misleading because it needs calibration by a supplementary method.[28] For the determination of more precise values of the PPXC *d*, a surface profilometer was used. As shown in Figure 3, all of the samples were quite flat (except for the area near the edge of the films) with little variation in thickness. Table I summarizes the *d* data measured by the surface profilometer.

Morphology of the Films

The effect of *d* on the surface morphology of PPXC was analyzed by AFM. Figure 4 shows the representative AFM micrographs of the samples, which showed features of structural change and grain growth for the PPXC films with various thicknesses, ranging from 0.32 to 120 μm.

In the AFM micrographs, grain features protruding from the film surface were obvious. The crystal grains were smaller and less definable (however, the number of them was larger); this produced a smoother surface, as shown in Figure 4(a). Then, the grains gradually became larger; this resulted in a rougher surface, as shown in Figure 4(b–e). As shown in some figures, especially Figure 4(d,e), the crystal grains were observed to have agglomerated together to form a smaller number of bigger grains. Clearly, the thicker PPXC films exhibited profounder grain features; this indicated that the grains grew with increasing *d*. These results could be attributed to the surface energy minimization during the growth process to achieve a thermodynamic equilibrium.[33] As the growth proceeded, those grains with a preferred growth direction survived because the surface tended to evolve toward a situation of low surface energy. This led to the evolution of a large-grained columnar morphology from a much greater number of fine grains, which originally nucleated on the substrate.[33]

Previous reports have shown that when the deposition is carried out under optimal conditions (fixed temperature and pressure), the roughness of the polymer film varied according to a power law depending on the thickness:[19,20,22]

$$\text{rms} = d^{\beta} \tag{1}$$

where β is an exponent that depends on the film growth process over time. In this study, rms of the samples was extracted from their AFM images. In Figure 5, the rms values versus the thickness (*d*) are plotted on a log–log plot.

In our study, the roughness as a function of *d* (from 320 to 120,000 nm) also obeyed the power law with $\beta = 0.240 \pm 0.005$. This thickness dependence of the film surface roughness could be explained by a nonstationary growth mechanism of the polymer; this suggested that unlike the case of semiconductors and metals deposited by physical vapor deposition, which show a steady growth atom by atom and layer by layer, the diffusion of the monomers and the relaxations of polymer chains played crucial roles in the evolution of the surface morphology according to *d* during the CVD process.[19,22,34]

Film Crystallinity and Crystal Structure as Determined by XRD Analysis

As shown in Figure 6, the room-temperature XRD peaks for the PPXC films with different thicknesses were obtained to study their crystallinity and crystal structures.

The major diffraction peak at a 2θ value of about 11° derived from the (020) plane of the monoclinic unit cell; this crystal phase is referred to as the α phase.[35–37] The major diffraction peaks of all of the samples almost stood at the same angle position; this indicated that nearly no change in the (020) plane spacing occurred as *d* increased. However, the peak intensity changed obviously. To make a detailed analysis, the XRD data was resolved by Jade 6.5 software (Rigaku Corp., Tokyo, Japan), which can simply estimate the crystallinity and average crystal size of the samples from the peak area and the full width at half-maximum (fwhm) of the reflection peak, respectively. Specifically, the software estimated the crystallite sizes or coherence lengths perpendicular to a particular crystallographic plane (L_{hkl}) with the Scherrer equation:[38]

$$L_{hkl} = \frac{0.9\lambda}{B\cos\theta} \tag{2}$$

where λ is the X-ray wavelength, B is the fwhm (rad) of the reflection peak, and θ is the diffraction angle. Table II lists the data of 2θ, fwhm, (020) plane spacing, and the estimated results of crystallinity and crystal size by the software. It is worth noting

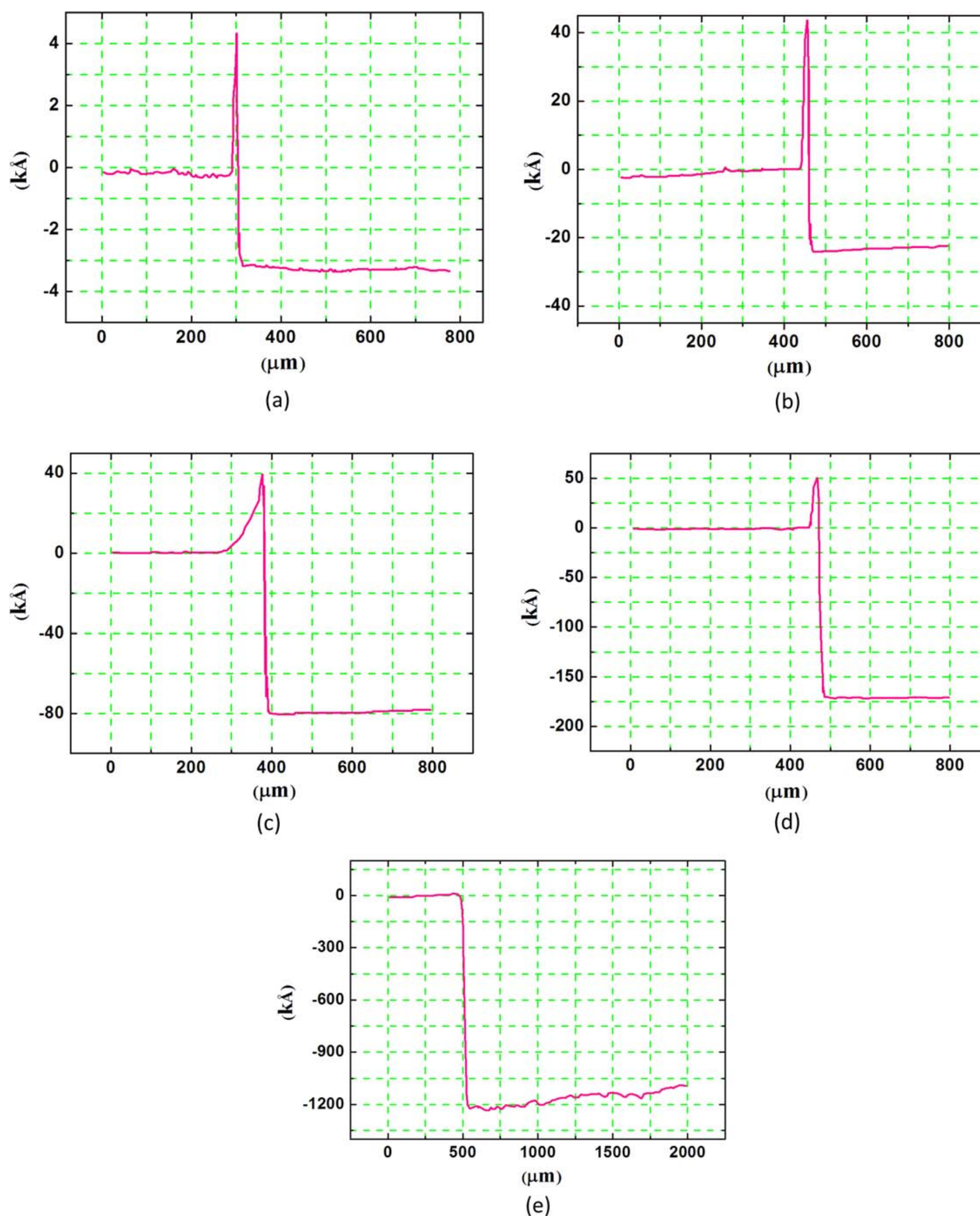

Figure 3. Surface profilometer analysis of the thickness of the PPXC films. [Color figure can be viewed in the online issue, which is available at wileyonlinelibrary.com.]

that these results were only used to compare the relative degree of crystallinity and crystal size and not the absolute values.

The (020) plane spacing of the PPXC films with different thicknesses was about 6.46 Å. This was consistent with the previous study by Murthy et al.[36] and suggested that the dimension *b* of the PPXC monoclinic unit cell was 12.8 Å. Nearly no change in the (020) plane spacing occurred as *d* increased; this was probably because all of the films were deposited under the same conditions (the same temperature, pressure, and substrate). It is also clear from Table II that both the crystallinity and crystal size increased

Table I. *d* Data Measured with a Surface Profilometer

Sample	*d* (μm)
a	0.32
b	2.39
c	7.98
d	17.11
e	120.00

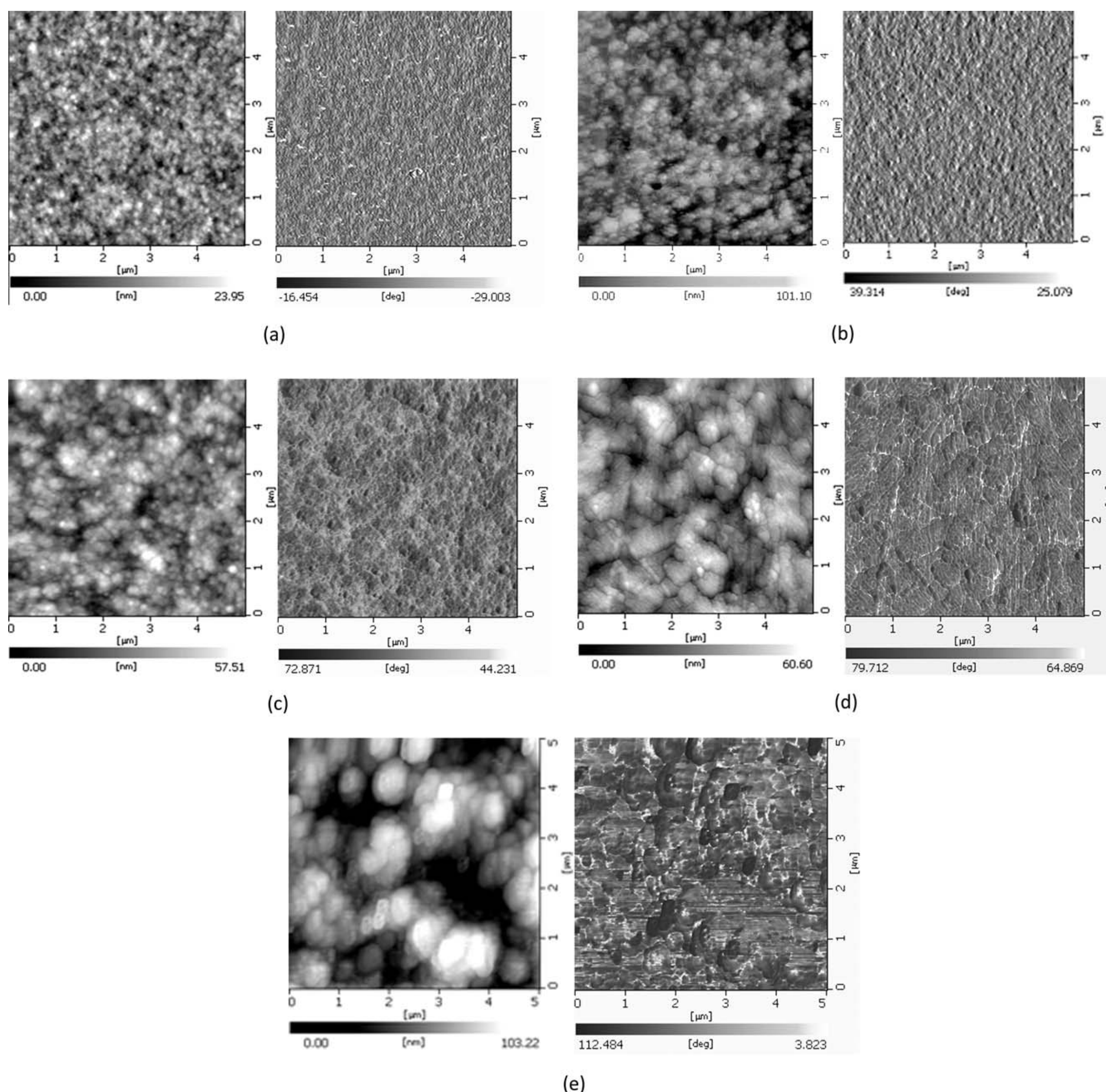

Figure 4. Evolution of the AFM images of PPXC films with different thicknesses: (a) 0.32, (b) 2.39, (c) 7.98, (d) 17.11, and (e) 120.00 μm. Height images are on the left, and phase images are on the right.

gradually as d changed from 0.32 to 120 μm. This agreed well with the AFM observations; above that value, the crystal grains grew larger as d increased. For this trend, one reasonable cause may have been that the surface confinement effect between the substrate and thin film was likely to retard the crystallization process of the polymers and result in a lower crystallinity and smaller crystal size in a thinner film.[21,22] In fact, the retardation of crystallization in the thin/ultrathin film has been observed for many polymeric film systems in previous studies.[26,39]

Crystal Orientation Behavior of the Films

Before the discussion about crystal orientation in the films, it is helpful to give a brief introduction to the two typical preferential orientations of crystal lamellae in polymers. In general, semicrystalline polymers can crystallize on a substrate, whereby molecular chains fold back and forth into stems to form crystal lamellae. As shown in Figure 7, two preferred polymer lamellae orientations are commonly encountered: (1) edge-on lamellae, in which the fold surface is perpendicular to the substrate and the molecular chain axis is parallel to the substrate, and (2) flat-on lamellae, in which the fold surface is parallel to substrate and the molecular chain axis is normal to the substrate.

As shown in Figure 6, the (020) peak dominated the XRD diffraction pattern of the samples; this indicated that most of the (020) crystal planes in the films were parallel to the substrate. Because the α phase of PPXC was a monoclinic unit cell and it was similar to the α phase of PPX in that the polymer chains

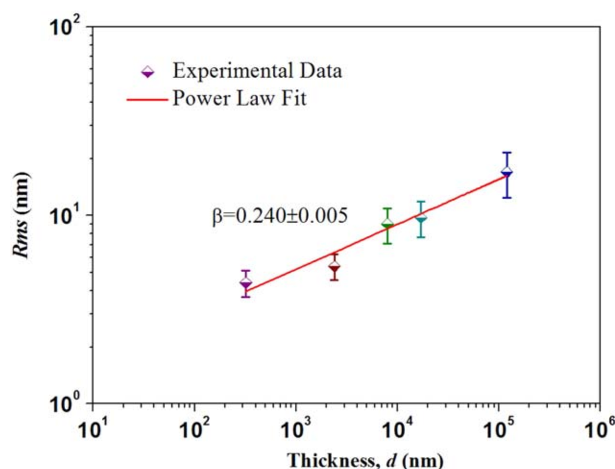

Figure 5. rms values of the PPXC films (from AFM scans) as a function of *d*. [Color figure can be viewed in the online issue, which is available at wileyonlinelibrary.com.]

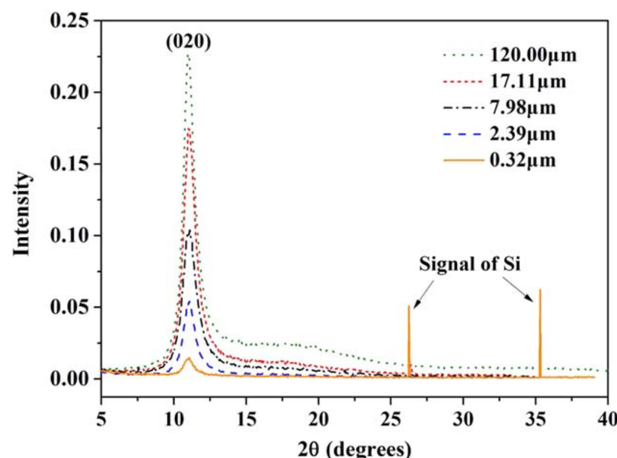

Figure 6. Room-temperature XRD patterns of the PPXC films with different thicknesses. [Color figure can be viewed in the online issue, which is available at wileyonlinelibrary.com.]

were in the *c* direction,[36] the orientation relationship between the crystal and substrate can be represented as shown in Figure 8. The molecular orientation in the films was nominally parallel to the substrate; this means that the edge-on lamellae should have existed in the PPXC samples. Although few studies have previously discussed the crystal orientation of PPXC, the crystallization of PPX during polymerization has been well studied, and many researchers have concluded that the as-deposited PPX films were mainly composed of folded chain crystals, which were edge-on oriented on the substrates.[25,40,41] In fact, the edge-on oriented crystal lamellae in the films were thermodynamically favored according to a simple model proposed by Wang et al.;[42] this suggested that when the polymer film is not very thin, the growth of edge-on crystal lamellae can minimize the increase in new interfacial area, and thus, the interfacial energy increases. This was also consistent with the previous observations by AFM that the films showed a columnar grain surface morphology.

Certainly, the unique edge-on crystal orientation shown in Figure 8 is an ideal situation. In reality, the normal to (020) planes will not be always perpendicular to the substrate. Therefore, the study of the crystal orientation distribution provided a more complete picture of the microstructures of these PPXC thin films. Various techniques exist for this purpose; however, the X-ray pole figure is the most suitable one for this study because it is quantitative, nondestructive, and especially suitable for the sample on a substrate. As introduced previously, to perform an X-ray pole figure scan with the Schultz reflection method, two operations are needed: (1) sample tilting from 0 to 90° (χ) and (2) sample rotation from 0 to 360° (φ). In this study, however, the second operation was unnecessary because the films were deposited on the substrate without being drawn in any direction; the azimuthal distribution of the crystallites should have been random. Figure 9 shows the wide-angle XRD pattern of the PPXC film (120 μm), which was recorded with the beam normal to the sample surface. The almost isotropic rings with the same radius and relative intensities demonstrated that there was relatively little preferred azimuthal orientation within the PPXC film.

Figure 10 shows the X-ray pole figure data of the PPXC films with different thicknesses. The (020) plane diffraction intensity versus the sample χ was plotted. Because the samples were azimuthally isotropic, the X-ray pole figure data could be represented as a three-dimensional plot through rotation about the intensity axis from 0 to 360° (φ). As shown in Figure 11, the PPXC films evidently exhibited a typical single-fiber texture structure; the rotational axis, which also corresponded to the Si substrate normal (Z), was the fiber axis.

As shown in Figures 10 and 11, the intensity peak of the (020) plane became sharper as the samples grew thicker; this implied

Table II. Data Summary of the XRD Analysis of the PPXC Films with Different Thicknesses

d (μm)	2θ (°)	fwhm (°)	(020) plane spacing (Å)	Crystal size (Å)	Crystallinity (%)[a]
0.32	11.05	1.19	6.461	55	12
2.39	11.10	1.10	6.458	59	19
7.98	11.10	0.91	6.458	71	29
17.11	11.05	0.77	6.461	84	41
120.00	11.00	0.72	6.463	89	47

[a] The crystallinity was normalized by the penetration depth of the X-ray, which was assumed to be 1 μm in this study.

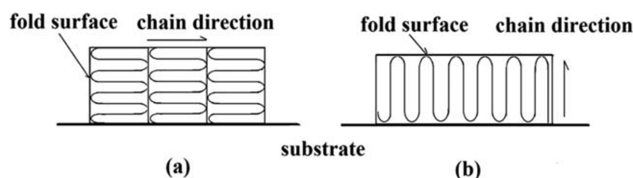

Figure 7. Two typical preferential orientations of crystal lamellae in the polymer films: (a) edge-on and (b) flat-on lamellae.

that the (020) fiber texture was enhanced as d increased. To confirm this trend, we used the Herman's orientation function (f_H), an average index of the orientation order, which can provide a quantitative analysis of the preferred orientation order. According to its definition[43]

$$f_H = \frac{3 < \cos^2 \chi_{(hld,z)} > -1}{2} \tag{3}$$

where $\chi_{(hkl,Z)}$ is the angle between the axis normal to the (hkl) planes and a reference axis Z (in the case here, Z was normal to the substrate or film surface). The average mean square cosine value is related to the rotation and tilt intensity scans by the following equations:[30,44]

$$<\cos^2 \chi_{(hld,Z)}> = \frac{\int_0^{\frac{\pi}{2}} I(\chi_{(hkl,Z)}) \cos^2 \chi_{(hkl,Z)} \sin \chi_{(hkl,Z)} d\chi_{(hkl,Z)}}{\int_0^{\frac{\pi}{2}} I(\chi_{(hkl,Z)}) \sin \chi_{(hkl,Z)} d\chi_{(hkl,Z)}} \tag{4}$$

$$I(\chi_{(hkl,Z)}) = \int_0^{2\pi} I(\chi_{(hkl,Z)}, \varphi) d\varphi \tag{5}$$

where $I(\chi_{(hkl,Z)})$ is the dependence of the intensity of the (hkl) reflection on the orientation angle recalculated from the azimuthal angle by eq. (5). Here, we chose the strongest (020) reflection. So, the (020) intensity distribution first needed to be integrated over φ from 0 to 2π and then integrated over χ from 0 to $\pi/2$. On the basis of the data in Figure 10, the f_H values of the samples could be calculated by use of eqs. (3–5). The results are listed in Table III.

The values in Table III could be compared to a perfectly oriented sample ($f_H = 1$), where the normal to the (020) diffraction planes was strictly parallel to the reference axis Z (the fiber axis), that is, the extreme edge-on oriented crystal lamellae, to random orientation $f_H = 0$, and to $f_H = -0.5$, where the normal to the (020) planes is strictly perpendicular to the fiber axis Z, that is, the extreme flat-on oriented crystal lamellae. As shown in Table III, the value of f_H increased from 0.293 to 0.541 as d grew from 0.32 to 120 μm; this indicated that stronger (020) fiber texture structures with a higher degree of edge-on orientation order existed in the thicker PPXC films. In other words, as the films grew thicker, a higher concentration of edge-on lamellae could be found in them. Although the simple thermodynamic model by Wang et al.[42] could explain why the edge-on lamellae were preferred in the sample, it was insufficient to describe the increase of the fraction of edge-on lamellae with increasing d.

It has previously been reported that many factors, such as the sample preparation methods, solvent, crystallization temperature, and surface interactions, can affect the lamellar orientation

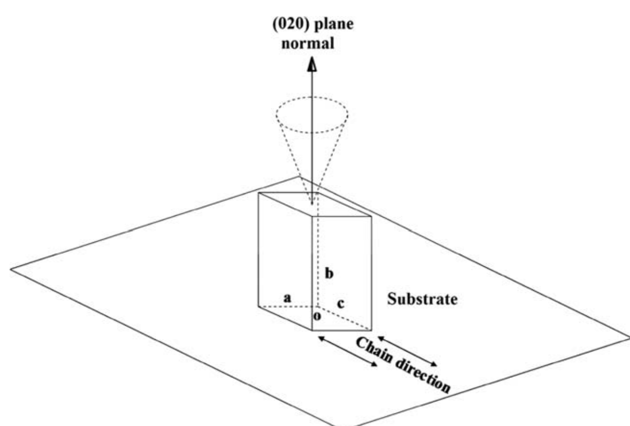

Figure 8. Illustration of the ideal orientation relationship between the crystal unit cell and the substrate.

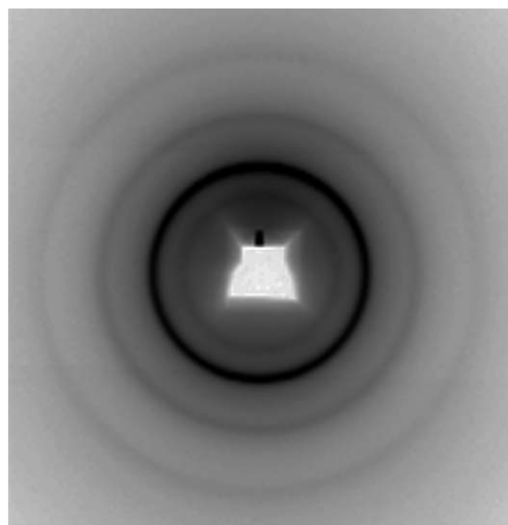

Figure 9. Wide-angle XRD pattern of the PPXC film (120 μm) with the beam perpendicular to the sample surface.

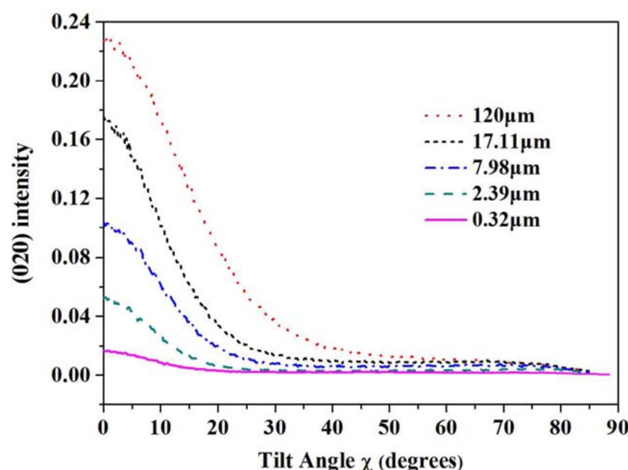

Figure 10. (020) intensity distribution of the PPXC films with different thicknesses. [Color figure can be viewed in the online issue, which is available at www.interscience.wiley.com.]

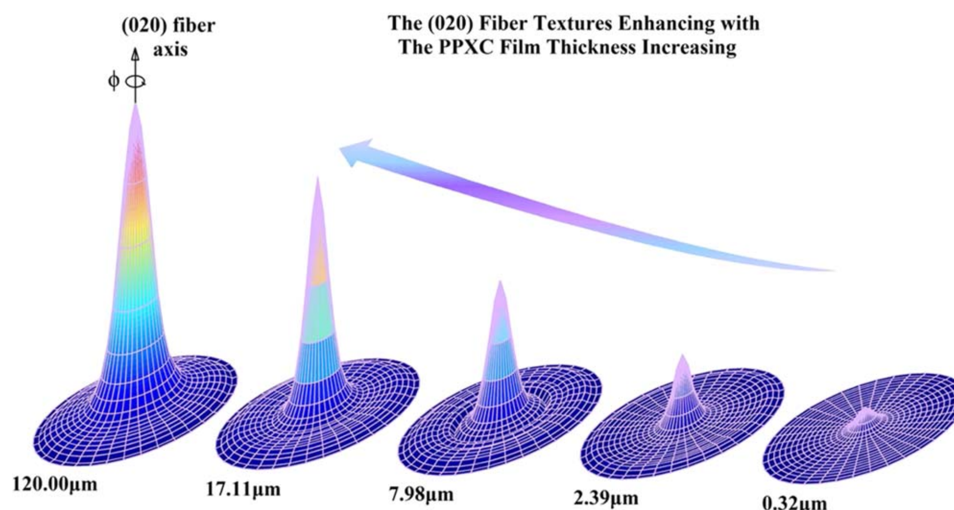

Figure 11. Three-dimensional representation of the (020) intensity distribution of the PPXC films with different thicknesses. [Color figure can be viewed in the online issue, which is available at wileyonlinelibrary.com.]

in polymeric films.[45] As the samples in this study were deposited on the same Si substrate under constant conditions, this *d* dependence of the crystal orientation order in the films should have been relevant to the interactions between the polymer chains and the substrate (the strength of the interactions should have increased with the reduction of *d*). In this study, actually, the strength of the interactions was not weak because of the fact that the PPXC films adhered extremely well to the Si surface (only the thick samples were successfully peeled off the substrate). When the film was very thin, the strong interactions (adhesion effect) between the polymer film and the substrate severely retarded the motion of the polymer chains. In this case, it was difficult for the chains to fold upward to form edge-on lamellae; thus, the nucleation of flat-on lamellae was preferred near the polymer/substrate interface. As the film grew thicker, the interactions between the polymer chains and the substrate became weaker; the polymer chains, which had a higher mobility, exhibited a stronger tendency to orient with their longest dimension parallel to the film surface.[46] Consequently, a higher concentration of edge-on lamellae arose in the thicker film. In a word, we believe that in this study, the *d* dependence of the crystal orientation behavior of the PPXC films was associated with the strong adhesion on the film/substrate interfaces.

CONCLUSIONS

In this study, several PPXC films with thicknesses ranging from 10^2 nm to 10^2 μm were deposited on Si substrates by the CVD method under the same conditions. With AFM, XRD, and X-ray pole figure characterizations, we found that the *d* influenced the morphology, crystal structure, and crystal orientation behavior of the PPXC films.

Table III. f_H Values of the PPXC Films with Different Thicknesses

d	0.32 μm	2.39 μm	7.98 μm	17.11 μm	120.00 μm
f_H	0.293	0.302	0.379	0.454	0.541

The surface morphology probed by AFM showed a power law dependence of the surface roughness as a function of *d;* this suggested that the diffusion of the monomers and the relaxations of the polymer chains were the main factors governing the evolution of the surface morphology according to *d*.

Because the surface confinement effect on the film/substrate interfaces retarded the polymer crystallization process, the XRD results indicated that both the crystallinity and crystal size of the PPXC films decreased as *d* decreased.

The X-ray pole figure revealed that the (020) fiber texture structures with the *b* axis of the crystal unit cell parallel to the Si substrate normal existed in the PPXC films. These fiber textures, which were mainly composed of edge-on crystal lamellae, were thermodynamically favored because the growth of edge-on crystal lamellae in the film minimized the new interfacial area increase and, thus, the interfacial energy increase. f_H increased as *d* increased; this indicated that stronger (020) fiber texture structures with a higher concentration of edge-on lamellae existed in the thicker PPXC films; this thickness dependence of the crystal orientation behavior was interpreted as caused by the strong adhesion effect between the polymer chains and the substrate.

ACKNOWLEDGMENTS

The authors thank Zhang Xinmin (SSRF) for assistance with the X-ray pole figure data collection. This study was supported by the National Natural Science Foundation of China (contract grant number 51173173).

REFERENCES

1. Gorham, W. F. *J. Polym. Sci. Part A1: Polym. Chem.* **1966**, *4*, 3027.
2. Tanioka, A.; Fukushima, N.; Hasegawa, K.; Miyasaka, K.; Takahashi, N. *J. Appl. Polym. Sci.* **1994**, *54*, 219.
3. Yamagishi, F. G. *Thin Solid Films* **1991**, *202*, 39.
4. Murarka, S. P. *Solid State Technol.* **1996**, *39*, 83.

5. Song, J. S.; Lee, S.; Jung, S. H.; Cha, G. C.; Mun, M. S. *J. Appl. Polym. Sci.* **2009**, *112*, 3677.
6. Beach, W. F. Encyclopedia of Polymer Science and Technology; Wiley: Hoboken, NJ, **2004**.
7. Schmidt, E. M.; Bak, M. J.; Christensen, P. *J. Neurosci. Methods* **1995**, *62*, 89.
8. Wright, D.; Rajalingam, B.; Karp, J. M.; Selvarasah, S.; Ling, Y.; Yeh, J.; Langer, R.; Dokmeci, M. R.; Khademhosseini, A. *J. Biomed. Mater. Res. A* **2008**, *85*, 530.
9. Chang, T. Y.; Yadav, V. G.; De Leo, S.; Mohedas, A.; Rajalingam, B.; Chen, C.-L.; Selvarasah, S.; Dokmeci, M. R.; Khademhosseini, A. *Langmuir* **2007**, *23*, 11718.
10. Zoumpoulidis, T.; Prodromakisy, T.; Van Zeijl, H.; Michelakisy, K.; Bartek, M.; Toumazou, C.; Dekker, R. Sensors, 2009; IEEE: Christchurch, **2009**, pp 7–12.
11. Po-Jui, C.; Rodger, D. C.; Saati, S.; Humayun, M. S.; Yu-Chong, T. *J. Microelectromech. Syst.* **2008**, *17*, 1342.
12. Ganguli, S.; Agrawal, H.; Wang, B.; McDonald, J. F.; Lu, T. M.; Yang, G.; Gill, W. N. *J. Vac. Sci. Technol. A* **1997**, *15*, 3138.
13. Zhang, X.; Dabral, S.; Chiang, C.; McDonald, J. F.; Wang, B. *Thin Solid Films* **1995**, *270*, 508.
14. Senkevich, J. J.; Desu, S. B. *Polymer* **1999**, *40*, 5751.
15. Senkevich, J. J.; Desu, S. B.; Simkovic, V. *Polymer* **2000**, *41*, 2379.
16. Treiber, G.; Boehlke, K.; Weitz, A.; Wunderlich, B. *J. Polym. Sci. Polym. Phys. Ed.* **1973**, *11*, 1111.
17. Iwamoto, R.; Bopp, R. C.; Wunderlich, B. *J. Polym. Sci. Polym. Phys. Ed.* **1975**, *13*, 1925.
18. Biscarini, F.; Samorí, P.; Greco, O.; Zamboni, R. *Phys. Rev. Lett.* **1997**, *78*, 2389.
19. Zhao, Y. P.; Fortin, J. B.; Bonvallet, G.; Wang, G. C.; Lu, T. M. *Phys. Rev. Lett.* **2000**, *85*, 3229.
20. Lee, I. J.; Yun, M.; Lee, S.-M.; Kim, J.-Y. *Phys. Rev. B* **2008**, *78*, 115427.
21. Huang, H.; Xu, Y.; Low, H. Y. *Polymer* **2005**, *46*, 5949.
22. Kahouli, A. *J. Appl. Phys.* **2012**, *112*, 064103.
23. Flesch, H.-G.; Werzer, O.; Weis, M.; Jakabovič, J.; Kováč, J.; Haško, D.; Jakopič, G.; Wondergem, H. J.; Resel, R. *Phys. Status Solidi. A* **2009**, *206*, 1727.
24. Wei, L.; Parhi, P.; Vogler, E. A.; Ritty, T. M.; Lakhtakia, A. *Mater. Lett.* **2010**, *64*, 1063.
25. You, L.; Yang, G.; Knorr, D. B.; McDonald, J. F.; Lu, T. M. *Appl. Phys. Lett.* **1994**, *64*, 2812.
26. Frank, C. W.; Rao, V.; Despotopoulou, M. M.; Pease, R. F. W.; Hinsberg, W. D.; Miller, R. D.; Rabolt, J. F. *Science* **1996**, *273*, 912.
27. Han, H.-C.; Chang, Y.-R.; Hsu, W.-L.; Chen, C.-Y. *Biosensors Bioelectron.* **2009**, *24*, 1543.
28. Lee, G.-Y.; Ko, H.; Jung, H.-W.; Ye, S.-J.; Kim, M.-H.; Pyun, J.-C. *Proc. Eng.* **2011**, *25*, 321.
29. Schulz, L. G. *J. Appl. Phys.* **1949**, *20*, 1030.
30. Alexander, L. E. X-ray Diffraction Methods in Polymer Science; Wiley-Interscience: New York, **1969**.
31. Cullity, B. D.; Stoc, S. R. Elements of X-Ray Diffraction, 3rd ed.; Prentice Hall: Upper Saddle River, New Jersey, **2001**.
32. Kasai, N.; Kakudo, M. X-ray Diffraction by Macromolecules; Springer: Berlin, **2005**; p 239.
33. Vaeth, K. M.; Jackman, R. J.; Black, A. J.; Whitesides, G. M.; Jensen, K. F. *Langmuir* **2000**, *16*, 8495.
34. Lai, Z. W.; Das Sarma, S. *Phys. Rev. Lett.* **1991**, *66*, 2348.
35. Isoda, S.; Kawaguchi, A.; Katayama, K.-I. *J. Polym. Sci. Polym. Phys. Ed.* **1984**, *22*, 669.
36. Murthy, N. S.; Kim, H.-G. *Polymer* **1984**, *25*, 1093.
37. Iwamoto, R.; Wunderlich, B. *J. Polym. Sci. Polym. Phys. Ed.* **1973**, *11*, 2403.
38. Scherrer, P.; Stoll, P. Z. *Anorg. Allg. Chem.* **1922**, *121*, 319.
39. Jeon, K.; Krishnamoorti, R. *Macromolecules* **2008**, *41*, 7131.
40. Kubo, S.; Wunderlich, B. *J. Appl. Phys.* **1971**, *42*, 4558.
41. Niegisch, W. D. *J. Appl. Phys.* **1967**, *38*, 4110.
42. Wang, Y.; Ge, S.; Rafailovich, M.; Sokolov, J.; Zou, Y.; Ade, H.; Lüning, J.; Lustiger, A.; Maron, G. *Macromolecules* **2004**, *37*, 3319.
43. Hermans, J. J.; Hermans, P. H.; Vermaas, D.; Weidinger, A. *Recl. Trav. Chim. Pays-Bas.* **1946**, *65*, 427.
44. Kołbuk, D.; Sajkiewicz, P.; Maniura-Weber, K.; Fortunato, G. *Eur. Polym. J.* **2013**, *49*, 2052.
45. Liu, Y.-X.; Chen, E.-Q. *Coord. Chem. Rev.* **2010**, *254*, 1011.
46. Wang, Y.; Chan, C.-M.; Ng, K.-M.; Li, L. *Macromolecules* **2008**, *41*, 2548.